

Antimony(III) Dithiocarbamates: Synthesis, Spectral, Theoretical and Biological Activities

S. TAMILVANAN¹

Department of Chemistry, Annamalai University, Annamalainagar-608002, India

Corresponding author: E-mail: laksuntam@gmail.com

Received: 10 September 2021;

Accepted: 13 November 2021;

Published online: 20 April 2022;

AJC-20756

Antimony(III) dithiocarbamate complexes *tris*(N,N-difurfuryldithiocarbamato-S,S')antimony(III) (**1**) and *tris*(N-furfuryl-N-(2-phenylethyl)dithiocarbamato-S,S')antimony(III) (**2**) have been synthesized and characterized by CHN analysis, FT-IR, ¹H NMR, ¹³C NMR spectra and antimicrobial studies. The characteristic thioureide ν(C-N) bands occur at 1459 and 1469 cm⁻¹ for complexes **1** and **2**, respectively. ¹H NMR and ¹³C NMR chemical shifts have been calculated using GIAO approach and the calculated chemical shifts shows good agreement with experiential shifts. The computational calculations of the antimony(III) complexes have been carried out by DFT/B3LYP using LANL2DZ basis set. The FMOs, MEP, Mulliken charge distribution and chemical activity parameters were calculated at the same level of theory. The antimicrobial activities of the antimony(III) complexes were assayed at the concentrations 400 and 800 μg/mL against four bacterial (*Vibrio cholera*, *Staphylococcus aureus*, *Klebsiella pneumoniae* and *Escherichia coli*) and two fungal species (*Candida albicans* and *Aspergillus niger*) by Agar-well disc diffusion method.

Keywords: Dithiocarbamate, Antimony(III), Molecular orbital theory, Antimicrobial activity.

INTRODUCTION

Dithiocarbamates are organosulfur ligands, which are form stable complexes with metal ions [1]. The two types of dithiocarbamates are formed based on the nature of amines used through the synthesis of the complex [2]. Chemistry of dithiocarbamates could be dated to begin in the early 20th century [3]. Commercial application of dithiocarbamate was used as a fungicide for the 1st time during World War-II. Other applications can be seen in the fields of acting as flotation agents, accelerating vulcanization, protecting radiators, biology, medicine, agriculture (pesticide), materials science, photo-stabilizing polymers and organic syntheses [4,5].

Metal dithiocarbamate complexes have been generally used as antibacterial agents. Derivatives of piperidine [6], saccharin [7], imidazole [8], piperazine [9], propanolol [10] and pyrrolidine dithiocarbamates have been synthesized and analyzed for their antibacterial effectiveness. The antibacterial activity of the dithiocarbamates is caused by their interference with necessary metabolic process in the cells [11]. Furthermore, dithiocarbamate complexes are also used as antifouling [12], herbicidal [13], growth depressant [14], anthelmintic [15],

biocidal [16], antioxidant [17], antiparkinson [18] and anti-radiation agents [19]. The antimycobacterial action of dialkyl-dithiocarbamate and pyrrolidinedithiocarbamate derivatives have been established [20]. Metal dithiocarbamate complexes such as molybdenum, lead, copper, zinc, cerium, bismuth and antimony dithiocarbamate complexes have been carefully studied in tribology [21]. Sarin *et al.* [22] studied and compared the antiwear performance of different dithiocarbamates of Mo, Pb, Zn, Bi and Sb. The antiwear propensity of these compounds is lined in the following order: Pb > Bi > Sb > Zn > Mo.

Generally, dithiocarbamates exist in three dissimilar resonant forms, as displayed in Fig. 1. In the resonant structure of dithiocarbamate forms A and C, there is a single bond between the C-N atom, which favours the delocalization of -1 charge between the C and two S atoms. Thus, both resonance forms favour the stabilization of soft metals of low oxidation states. The resonance structure of dithiocarbamate form B is often referred to as the thioureide (C-N) form. Here, the lone pair electron on the nitrogen is delocalised, resulting in a double bond character between the N and C group. It is in this resonant form that hardest metals of higher oxidation states are stabilized. Hence, the terrific stability of dithiocarbamate is often

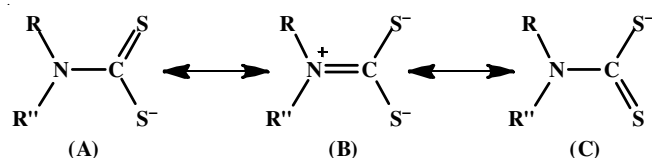


Fig. 1. Resonance structure forms of dithiocarbamate

due to the contribution of the resonance structure form B to the overall electronic structure of dithiocarbamate [23].

In this work, the synthesis of new antimony(III) dithiocarbamate complexes are reported. These novel synthesized complexes were characterized on the basis of CHN, IR, NMR and antimicrobial studies. Moreover, the IR and NMR spectral investigations of the both antimony complexes have been performed using DFT. Geometry optimization of structures were performed by DFT/B3LYP using LANL2DZ basis set with the Gaussian 09W package. In addition, HOMO-LUMO, Mulliken charge analysis and MEP analysis of information have been used to support the structural properties molecules.

EXPERIMENTAL

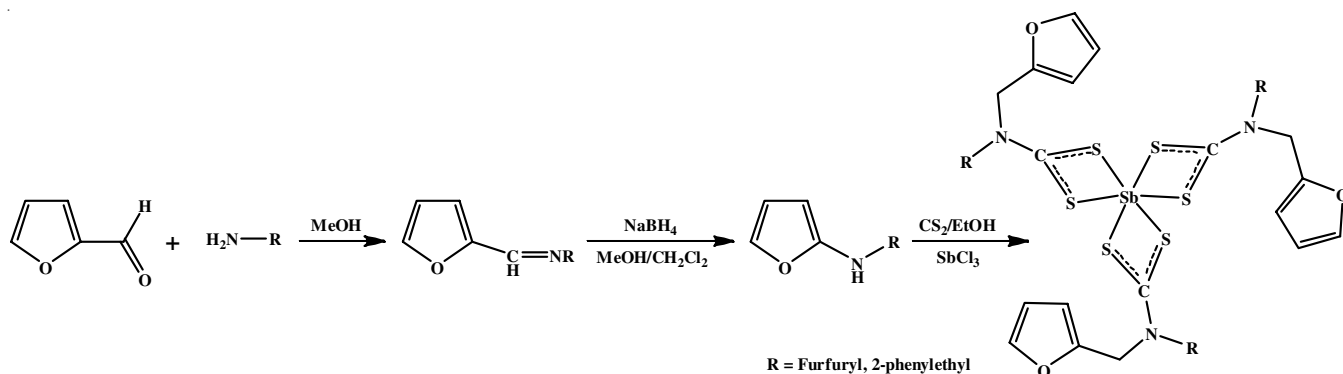
Antimony trichloride, the parent amines, reagents and the solvents were of analytical grade (commercially available) and used as supplied without further purification. Melting points of the complexes were determined with a thermal melting point apparatus and used with open capillary tubes. Elemental analyses (C, H & N) were carried out with an Elementar Analyse system GmbH Vario El V3.00 at Sophisticated Analytical Instrument Facility Centre, CDRI, Lucknow, India. FT-IR spectra were recorded on Thermo SHIMADZU FT-IR spectrophotometer (4000-400 cm^{-1}) as KBr pellets of the complexes. ^1H NMR and ^{13}C NMR spectra were recorded on a BRUKER 400 MHz spectrometer model at room temperature using CDCl_3 as solvent. The Bruker spectrometer performed at 400 MHz for ^1H NMR spectra and 100 MHz for ^{13}C NMR spectra. Trimethyl silane (TMS) as an internal reference for ^1H & ^{13}C NMR spectra.

Synthesis of secondary amines: Furfuraldehyde was added to primary amine (furfurylamine, 2-phenylethylamine) in MeOH and the mixture was stirred for 2 h. The solvent was removed. The resultant oily product was dissolved in methanol-dichloromethane (1:1) solvent mixture. To this solution, excess sodium borohydride (NaBH_4) was added very slowly at 5°C and stirred for 2 h. The reaction product was stirred for 12 h at

room temperature. After evaporation of the solvent, the resulting viscous liquid was washed with excess of water and dichloromethane was added in order to extract the product. Evaporation of the organic layer product was furfuryl based *sec*-amine [24].

Synthesis of tris(*N,N*-difurfuryldithiocarbamato-*S,S'*)antimony(III) (1): Furfuryl based *sec*-amine (furfurylamine) and carbon disulfide (CS_2) were dissolved in ethanol and stirred for 30 min under ice cold condition (5°C) to obtained a yellow dithiocarbamic acid. Antimony trichloride (SbCl_3) was added to the solution with constant stirring. Pale yellow solids were separated from the solution, which was filtered and washed with distilled water and dried in air [25]. The obtained product was recrystallized to get the good yield (**Scheme-I**). Yield: 80%, m.p.: 171°C . Anal. calcd. (found) % for $\text{C}_{33}\text{H}_{30}\text{N}_3\text{O}_6\text{S}_6\text{Sb}$ (*m.w.* 878.76): C, 45.10 (45.07); H, 3.44 (3.40); N, 4.78 (4.73). IR (KBr, ν_{max} , cm^{-1}): Experimental: 1459 $\nu(\text{C-N})$, 1012 $\nu(\text{C-S})$, 2854 $\nu(\text{C-H})$, Theoretical: 1436.54 $\nu(\text{C-N})$, 1019.11 $\nu(\text{C-S})$, 3229.06 $\nu(\text{C-H})$, ^1H NMR (400 MHz, CDCl_3 , ppm): Experimental: 5.10 (12H, s, CH_2 furfuryl); 6.37 (6H, H-4 (furyl); 6.43 (6H, H-3, (furyl); 7.40 (6H, H-5 (furyl): Theoretical: 4.6518 (23H) (CH_2 furfuryl); 6.2369 (33H) (6H, H-4 (furyl); 6.4805 (31H) (6H, H-3, (furyl); 7.2359 (34H) (6H, H-5 (furyl); ^{13}C NMR (100 MHz, CDCl_3 , ppm) Experimental: 48.3 (CH_2 furfuryl carbons); 110.0, 110.3, 142.1, 148.3 (furyl ring carbons); 204.1 (NCS_2): Theoretical: 50.4660 (22C) (CH_2 furfuryl carbons); 105.4785 (30C), 106.4727 (28C), 141.5118 (32C), 151.0340 (27C) (furyl ring carbons), 229.2841 (21C) (NCS_2).

Synthesis of tris(*N*-furfuryl-*N*-(2-phenylethyl)dithiocarbamato-*S,S'*)antimony(III) (2): Furfuryl based secondary amine (2-phenylethylamine) and carbon disulfide were dissolved in ethanol and stirred for 30 min under ice cold condition (5°C) to obtained a yellow dithiocarbamic acid. Antimony trichloride was added to the solution with constant stirring. Pale yellow solids were separated from the solution, which was filtered and washed with water and dried in air. The obtained product was recrystallized to get the good yield. Yield: 77%, m.p.: 158°C . Anal. calcd. (found) % for $\text{C}_{42}\text{H}_{42}\text{N}_3\text{O}_3\text{S}_6\text{Sb}$ (*m.w.* 950.95): C, 53.05 (53.01); H, 4.45 (4.43); N, 4.42 (4.39). Experimental: 1469 $\nu(\text{C-N})$, 1010 $\nu(\text{C-S})$, 2915 $\nu(\text{C-H})$. Theoretical: 1459.55 $\nu(\text{C-N})$, 1054.44 $\nu(\text{C-S})$, 3057.72 $\nu(\text{C-H})$. ^1H NMR (400 MHz, CDCl_3 , ppm) Experimental: 3.01 (6H, t, $\text{N-CH}_2\text{-CH}_2\text{-C}_6\text{H}_5$); 4.07 (6H, $\text{N-CH}_2\text{-CH}_2\text{-C}_6\text{H}_5$); 5.09 (6H,



Scheme-I: Reactions scheme for the synthesis of the antimony complexes

CH₂ furfuryl); 6.31-7.30 (aromatic protons). Theoretical: 2.1565 (34H) (6H, N-CH₂-CH₂-C₆H₅); 2.7201 (31H) (6H, N-CH₂-CH₂-C₆H₅); 3.3219 (35H) (6H, CH₂ furfuryl); 6.2633-7.4144 (42H) (40H) (75H) (69H) (74H) (73H) (71H) (43H) (aromatic protons); ¹³C NMR (100 MHz, CDCl₃, ppm) Experimental: 33.2 (N-CH₂-CH₂-C₆H₅); 50.1 (N-CH₂-CH₂-C₆H₅); 55.5 (CH₂ furfuryl); 110.6, 110.7, 142.5, 148.4 (furyl ring carbons); 126.2, 128.0, 128.6, 138.9 (phenyl ring carbons); 202.9 (NCS₂). Theoretical: 29.0222 (32C) (N-CH₂-CH₂-C₆H₅); 58.3779 (30C) (N-CH₂-CH₂-C₆H₅); 49.35266 (28C) (CH₂ furfuryl); 105.4327 (39C), 106.1780 (37C), 140.6455 (41C), 152.0503 (36C) (furyl ring carbons); 119.0206 (72C), 121.7775 (68C), 122.2451 (70C), 123.4992 (66C), 124.1583 (67C), (phenyl ring carbons); 226.9375 (27C) (NCS₂).

DFT computational studies: Geometry optimization of the complexes were performed by employing the DFT (density functional theory) at B3LYP (Becke 3-parameter exchange functional together with the Lee-Yang-Parr correlation functional) level and LANL2DZ basis set using the Gaussian 09W package [26]. However, the mainly optimized structural parameters such as bond distance, bond angle and dihedral angle were calculated from Gaussian 09W software package. The vibrational frequencies and molecular geometry optimization for the antimony complexes were calculated. Density functional theory is in good accuracy in reproduce the investigational values of molecular geometry. The ¹H NMR and ¹³C NMR spectra were performed using the GIAO [27,28] method using CDCl₃ solvent with TMS as reference. The molecular optimized structures of the complexes have been used to calculate the highest occupied molecular orbital (HOMO) and lowest unoccupied molecular orbital (LUMO) [29] images were visualized using Gauss View 5.0. Energy gap, electrophilicity, global hardness, Mulliken charge distribution of atoms [30] of systems were calculated using Gauss View 5.0. The nucleophilic and electrophilic regions were recognized by molecular electrostatic potential (MEP) was visualize using Gauss View 5.0 [31]. In addition, many other parameters like total energy, molecular dipole moment for the present antimony complexes have been also presented. Antimony(III) dithiocarbamate complexes were calculated on a personal laptop by using the Gaussian 09W software package.

Antimicrobial studies: The antimony complexes were screened for their *in vitro* antimicrobial (Bacteria: *Vibrio cholerae*, *Staphylococcus aureus*, *Klebsiella pneumoniae*, *Escherichia coli* and Fungi: *Candida albicans* and *Aspergillus niger*) activities by Mueller Hinton Agar-well diffusion method [32]. The sterile cork borer antibiotic disc (6 mm in diameter- three holes were made in each disc) loaded with required concentrations (400 and 800 µg/mL) of antimony complexes **1** and **2** were located on the spread plates. The cultures of the test microorganism were arranged in sterile nutrient broth medium and incubated at 37 °C for 24 h for bacteria and 27 °C for fungal, when inhibition or clear zones are detected in the region of each hole. The spread plates were incubated for 24 h. Afterwards, the zones of inhibition were examined and measured in millimeter as the activities against the tested pathogens. Ciprofloxacin was used as reference drug for comparison of microorganisms.

RESULTS AND DISCUSSION

Infrared analysis: Fourier-transform infrared (FT-IR) spectra of antimony dithiocarbamate complexes were recorded in the region 4000-400 cm⁻¹. The IR spectra of antimony dithiocarbamates features three distinguishing bands, mainly associated with the stretching vibrational bands. The ν(C-S) stretching vibration (1050-950 cm⁻¹) [33] is appeared as single bands for all the metal complexes and indicates a symmetrical bonding of the S atoms of the ligand to the central metal ion. The ν(C-N) (thioureide) stretching bands (1550-1450 cm⁻¹) of antimony dithiocarbamate complexes occurred as sharp bands. The ν(C-S) stretching vibrations bands are around 1012, 1011 cm⁻¹ in metal complexes **1**, **2** respectively, where as computational calculation bands at 1019.11 and 1059 cm⁻¹ using B3LYP theoretical method. For antimony dithiocarbamate complexes **1** and **2**, the thioureide (ν_{C-N}) bands are observed at 1459 and 1469 cm⁻¹, which where computationally calculated as 1436.54 and 1459.55 cm⁻¹, respectively. The shift in the vibrational bands of ν(C-N) by 15 cm⁻¹ upon complexation with a metal suggest a partial double bond character. The aromatic ν(C-H) bands are obtained in the range 2915-2854 cm⁻¹. This band is feature of NCS₂ band with an intermediary bond between single bond (1350-1250 cm⁻¹) [34] and double bond (1690-1640 cm⁻¹). The M-S stretching bands for antimony dithiocarbamate complexes usually in the region 400-300 cm⁻¹ and that could not be observed due to the infrared spectral range of the measurements. Infrared spectra of antimony dithiocarbamate complexes **1** and **2** are given in Fig. 2.

NMR analysis: ¹H & ¹³C NMR spectra of complexes **1** and **2** are given in Fig. 3. ¹H NMR spectra were characteristic of each dithiocarbamate ligand type. Thus, antimony complex **1** showed singlet observed at 5.10 ppm is assigned to CH₂ protons for furfuryl group, which were found the signal 4.6518 ppm based on the computational spectrum. The N-CH₂ (furfuryl) signals are shifted markedly downfield compared to the similar proton on the parent amine. The aromatic protons signals observed in the downfield in the range 6.37-7.40 ppm, which were theoretically observed in the region 6.2369-7.2359 ppm. The ¹H NMR spectrum of antimony complex **2**, shows an intense signal observed at 3.01 ppm due to the CH₂ protons of ethyl group of phenylethyl cluster moiety, which were theoretically observed at δ 2.1565 ppm. The N-CH₂ (phenyl ethyl) signals are shifted markedly downfield compared to the similar proton on the parent amine. The aromatic protons signals observed in the downfield regions in the range 6.31-7.30 ppm, which were theoretically observed in the regions 6.2633-7.4144 ppm.

The NCS₂ thioureide carbon signals are observed in the expected region (around δ 200 ppm) [35] for metal dithiocarbamate complexes. In complexes **1** and **2**, these signals are appeared at δ 204.1 ppm and δ 202.9 ppm due to the thioureide carbon using the gauge-invariant atomic orbital (GIAO) method, which were found at δ 229.2841 and δ 226.9378 ppm based on the theoretical spectra, respectively. The signal for CH₂ carbon of furfuryl appears at 48.3 and 55.5 ppm, which were theoretically obtained at δ 50.4660 ppm and δ 49.3526 ppm for complexes **1** and **2**, respectively. The remaining two signals

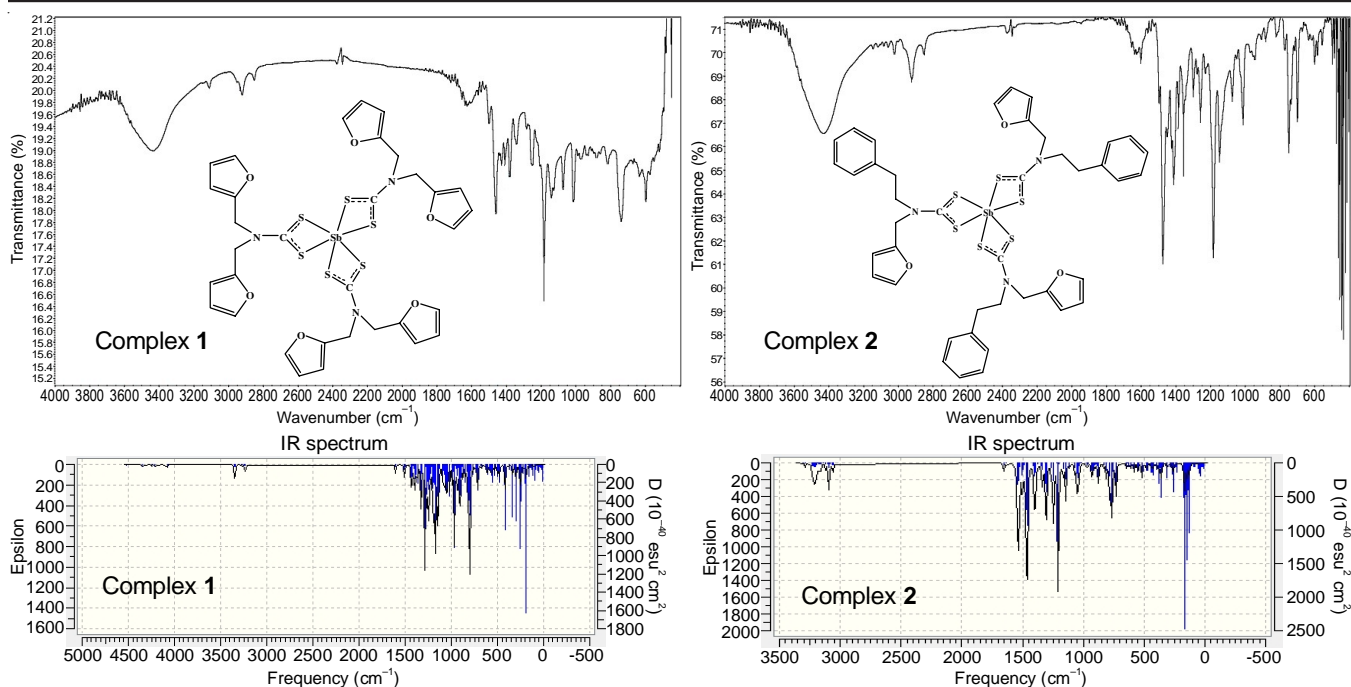


Fig. 2. Experimental (up) and computational (down) IR spectra of complexes **1** and **2**

in the aliphatic region (33.2 and 50.1 ppm) are assigned to ethylene carbons of phenyl ethyl group moiety. A downfield shift of CH₂ carbon signals compared to the similar carbons in the parent amine is an indication of the significant consequence of the complexation method,

Geometry of the molecule: The optimized molecular structure of the antimony dithiocarbamate complexes **1** and **2** are shown in Fig. 4. The selected bond lengths, bond angle and dihedral angle for the antimony dithiocarbamate complexes **1** and **2**. The C-N (thioureide) and C-S bond distances in the structure of dithiocarbamate complex **1** lies between 1.3517-1.3586 Å (C16-N9, C21-N10) and 1.75490-1.8294 Å (C16-S5, C16-S4), respectively. The bond angle and torsional angle of the complex **1** found at 65.59° (S4-Sb1-S5) and -176.42° (S6-C21-N10-C24), respectively. The C-N and C-S distances in the complex **2** lies between 1.3515-1.3552 Å (C19-N9, C27-

N10) and 1.7551-1.775 Å (C19-S5, C27-S7), respectively. The optimized structural parameters of dithiocarbamate complexes **1** and **2** are listed in Tables 1 and 2.

Frontier molecular orbitals (FMOs): The frontier molecular orbitals, the highest occupied molecular orbital (HOMO) and lowest unoccupied molecular orbital (LUMO) values and their differences can provide information about the reactivity of the molecule. It is used for analyzing thermal and optical properties of complexes. The most two significant orbitals in molecules for reactivity are two so-called FMOs (Frontier molecular orbitals). The FMOs play an important role in the optoelectronics properties [36], as well as in UV-vis spectra and quantum chemistry. Highest occupied molecular orbital is the highest energy that is still occupied, so actively it is the easiest to eliminate electrons from this orbital. HOMO acts as a Lewis base or it could be oxidation reaction. The other one

TABLE-1
OPTIMIZED STRUCTURAL PARAMETERS AT B3LYP/LANL2DZ BASIS SET FOR COMPLEX **1**

Bond distances (Å)		Bond angles (°)		Dihedral angles (°)	
S2-Sb1	2.81950	S2- Sb1-S3	63.89445	S6-C21-N10-C24	-176.42305
S3- Sb1	2.99582	S4- Sb1-S5	65.59214	S7-C21-N10-C22	-174.32413
S4- Sb1	2.61742	S6- Sb1-S7	64.59952	N10-C24-C56-C57	24.87666
S5- Sb1	3.04595	S3- C11-S2	118.9441	N10-C22-C27-C28	88.82917
S6- Sb1	2.79901	S3- C11-N8	121.9302	H35-C24-C56-C57	146.67701
S7- Sb1	2.95919	S2- C11-N8	119.1224	S2-C11-N8-C12	179.82365
C11-S2	1.80157	C12-N8- C14	114.6495	S3-C11-N8-C14	-178.92362
C11-S3	1.77491	S4- C16-S5	118.9980	N8-C12-C72-C73	-29.59920
C11-N8	1.35760	S4- C16-N9	117.7225	N8-C14-C48-C49	-97.40277
C16-S4	1.82947	S5- C16-N9	123.2793	H52-C49-C51-C53	178.92283
C16-S5	1.75496	C17-N9- C19	114.7384	S5-C16-N9-C17	-175.67476
C16-N9	1.35174	S6- C21-S7	119.1033	S4-C16-N9-C19	-178.99794
C21-S6	1.80659	S6- C21-N10	119.4289	N9-C17-C38-C39	-178.99794
C21-S7	1.76590	S7- C21-N10	121.4618	N9-C19-C64-C65	-97.93096
C21-N10	1.35865	C22-N10- C24	116.4043	H68-C65-C67-C69	178.81421

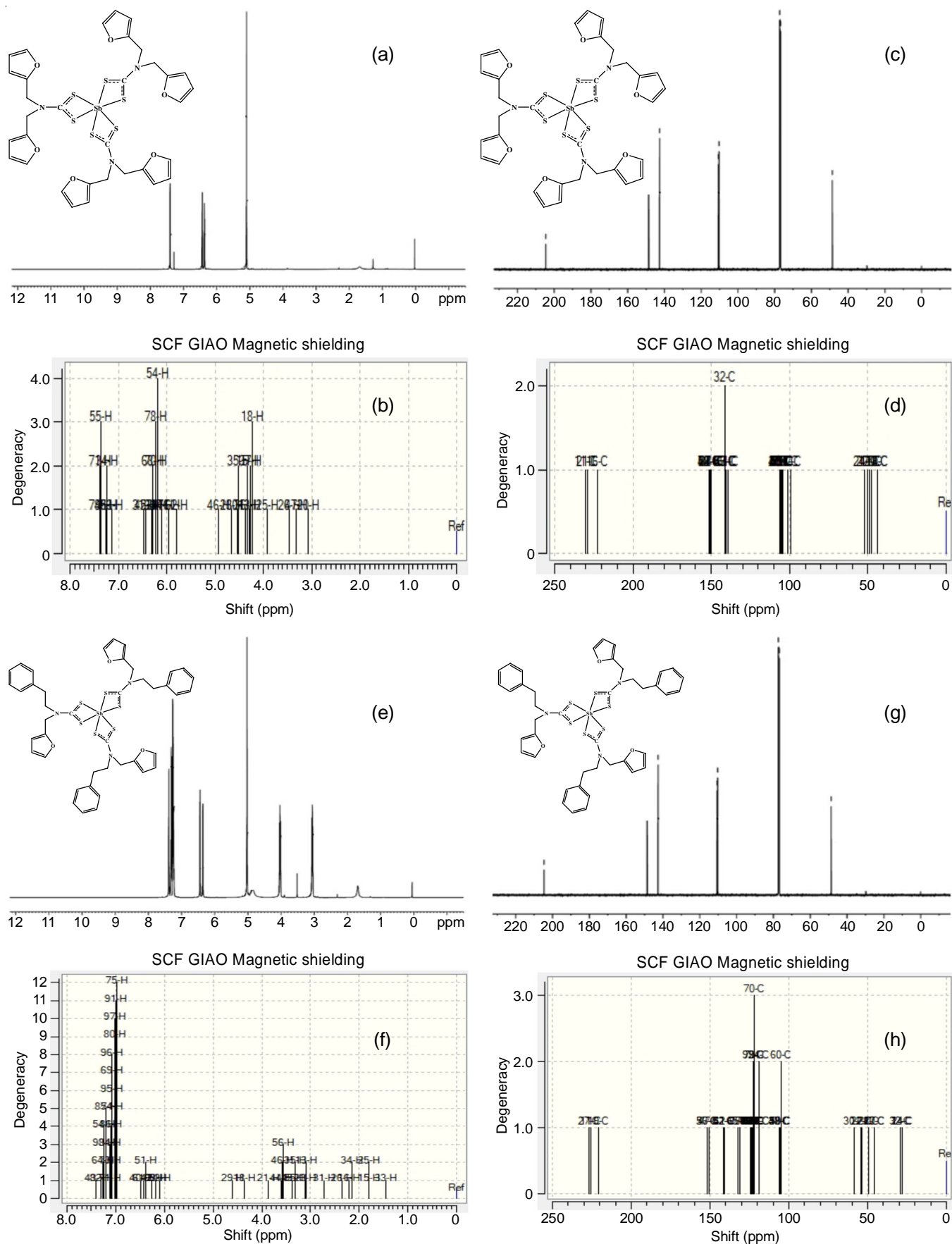


Fig. 3. Experimental (up) and computational (down) NMR spectra of complexes 1 and 2 [(a,b) - ^1H and (c,d) ^{13}C NMR for complex 1] [(e,f) - ^1H and (g,h) ^{13}C NMR for complex 2]

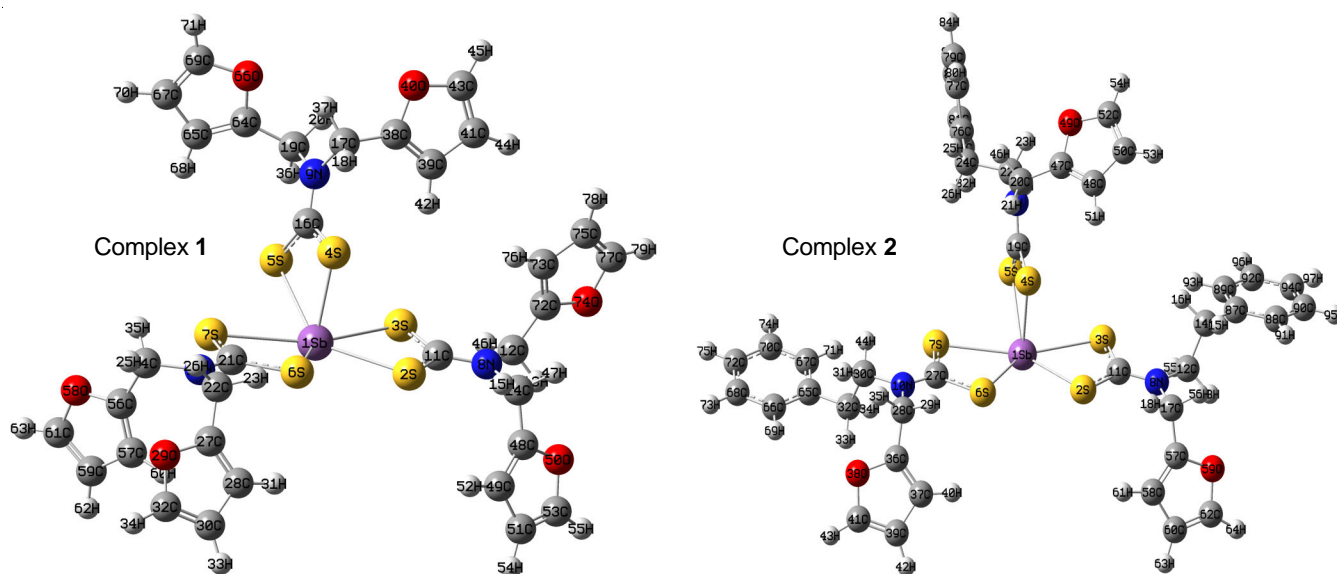


Fig. 4. Optimized structure with atoms numbering of complexes 1 and 2

TABLE-2
OPTIMIZED STRUCTURAL PARAMETERS AT B3LYP/LANL2DZ BASIS SET FOR COMPLEX 2

Bond distances (Å)		Bond angles (°)		Dihedral angles (°)	
S2-Sb1	2.80865	S2- Sb1-S3	64.49576	S6-C27-N10-C30	-177.56794
S3- Sb1	2.96468	S4- Sb1-S5	65.46160	S7-C27-N10-C28	-177.66670
S4- Sb1	2.61920	S6- Sb1-S7	64.32218	N10-C28-C36-C37	89.99315
S5- Sb1	3.05469	S3- C11-S2	118.8150	N10-C30-C32-C65	-178.85109
S6- Sb1	2.81264	S3- C11-N8	121.5189	H44-C30-C32-H33	-179.30427
S7- Sb1	2.97268	S2- C11-N8	119.6631	S2-C11-N8-C12	178.97129
C11-S2	1.80708	C12-N8- C17	115.2627	S3-C11-N8-C17	178.17167
C11-S3	1.77483	S4- C19-S5	119.1023	N8-C17-C57-C58	-92.34087
C11-N8	1.35333	S4- C19-N9	117.7621	N8-C12-C14-C87	-178.70990
C19-S4	1.82848	S5- C19-N9	123.1350	H15-C14-C12-H13	-177.44814
C19-S5	1.75518	C20-N9- C22	115.3623	S5-C19-N9-C20	177.78470
C19-N9	1.35153	S6- C27-S7	118.8028	S4-C19-N9-C22	177.23594
C27-S6	1.80612	S6- C27-N10	119.6801	N9-C20-C47-C48	-91.93560
C27-S7	1.77500	S7- C27-N10	121.5101	N9-C22-C24-C76	-178.97180
C27-N10	1.35521	C28-N10- C30	116.4530	H23-C22-C24-C26	-177.63648

is lowest unoccupied molecular orbital is the lowest lying orbital that is vacant, so energetically it is the easiest to add electrons into this orbital. LUMO acts as a Lewis acid or it could be reduction reaction.

Frontier molecular orbitals energy gap supports to identify the stability of structure. The calculated energy gap values 3.8125 and 3.8438 eV for complex 1 and 2, respectively. A molecule with a large energy gap is hard, less reactive and less polarizable whereas a molecule that possesses a small energy gap would be considered to be soft, more reactive and more polarizable [37]. The energy difference between the highest occupied molecular orbital and the lowest unoccupied molecular orbital can be used to determine the chemical hardness, polarizability, reactivity and softness values for a molecule. Other global descriptors calculated from the FMO energies, such as electrophilicity index and maximum charge transfer capability, electronic chemical potential, global hardness provide very useful information associated to the physical and physico-chemical properties. At this point, the smaller global

hardness and energy gap values mean the more reactive molecule; electrophilicity index in terms of the global hardness and electronic chemical potential represents the capability of the molecule to accept the electrons from a donor environment. The other significant parameters of the dithiocarbamate complex such as electronegativity (χ) and global softness (S), global hardness (η), electrophilicity (ω), chemical potential (μ), which have been effectively utilized to expect global chemical reactivity trends. These variables can be calculated from electron affinity (EA) and ionization potential (IP) values are showed in Fig. 5 and Table-3.

Ionization potential (IP) and electron affinity (EA) are related to the HOMO (ionization potential (IP) = $-E_{\text{HOMO}}$) and LUMO (electron affinity (EA) = $-E_{\text{LUMO}}$) energies, respectively, which are defined by Koopmans Theorem [38]. Fig. 5 and Table-3 reveals that the dithiocarbamate complex 1 has the highest ionization potential (IP) 5.9826 and electron affinity (EA) 2.1700 eV value, whereas dithiocarbamate complex 2 has the lowest ionization potential (IP) 5.9200 eV and electron

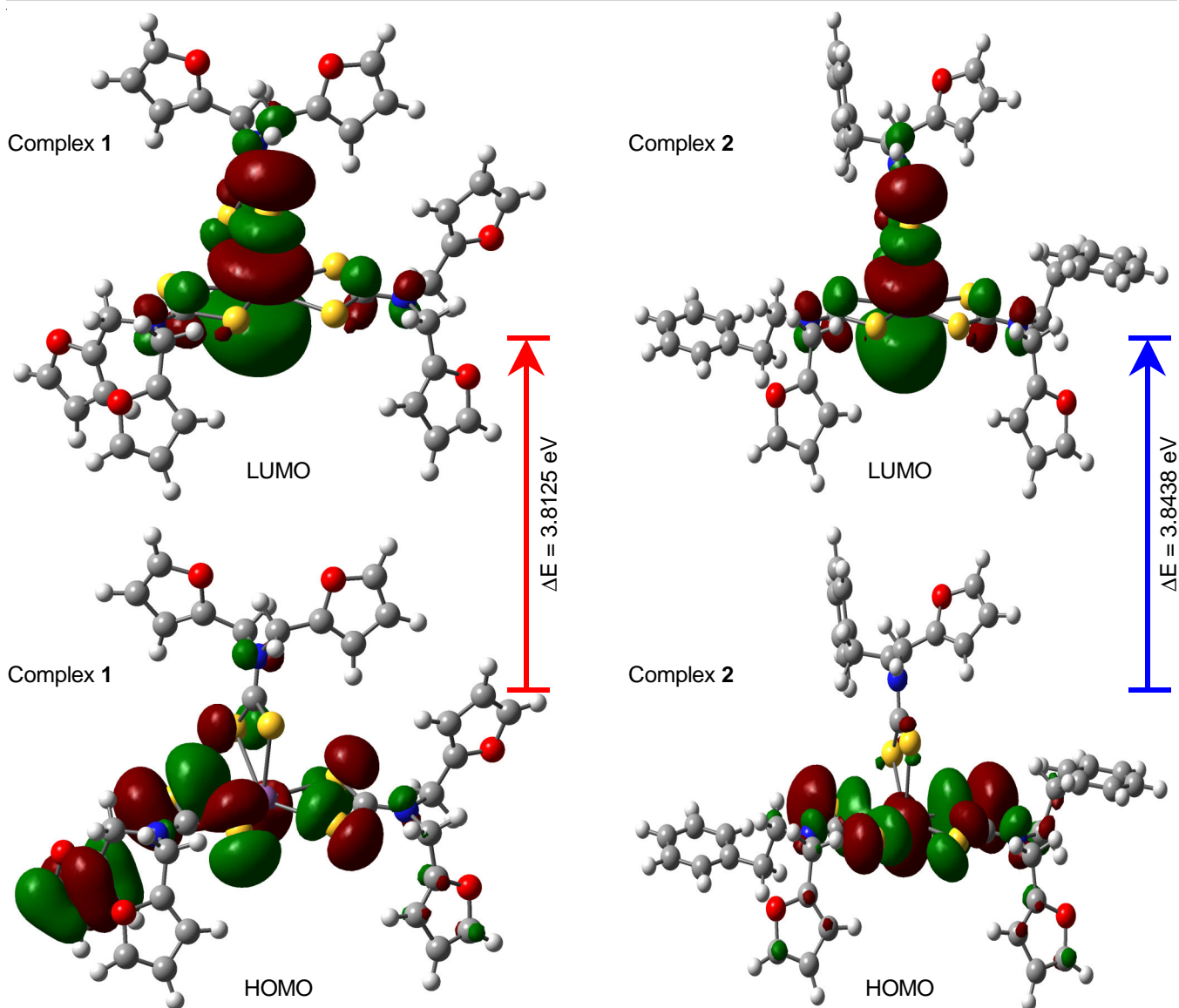


Fig. 5. HOMO, LUMO orbitals at the B3LYP/LANL2DZ basis set for complexes 1 and 2

TABLE-3 CALCULATED ENERGY VALUES OF COMPLEXES 1 AND 2		
Parameters	Complex 1 (eV)	Complex 2 (eV)
HOMO	-5.9826	-5.9200
LUMO	-2.1700	-2.0762
Energy gap	3.8125	3.8438
Ionization potential (IP)	5.9826	5.9200
Electron affinity (EA)	2.1700	2.0762
Global hardness (η)	1.9062	1.9219
Chemical potential (μ)	-4.0763	-3.9981
Electronegativity (χ)	4.0763	3.9981
Global softness (S)	0.2622	0.2602
Electrophilicity index (ω)	4.3584	4.1586
Energy	-1956.7736	-2081.3823
Dipole moment (Debye)	2.1651	3.0344

affinity (EA) 2.0762 eV value. These results correspond with the definitions of both properties of dithiocarbamate complexes, as they signify the negative values of E_{HOMO} and E_{LUMO} . The global hardness (η) and global softness (S) variables are defined

as [$\eta = \frac{1}{2} (E_{\text{LUMO}} - E_{\text{HOMO}}) = 1.9062 \text{ eV}$] and ($S = 1/2\eta = 0.2622 \text{ eV}$), respectively for the complex 1. The results reveals that dithiocarbamate complex 1 can be considered to be least polarisable, hardest and least reactive. Mulliken [39] defined electronegativity (χ) as [$\chi = -\frac{1}{2} (E_{\text{HOMO}} + E_{\text{LUMO}})$ 4.0763 eV, 3.9981 eV for complex 1 and 2, respectively) and this electronegativity represents the attraction of electrons by the actions of functional group and an atom, resultant in the transition of electronic charges from poor to richer electronegativity (χ) region within a molecule. As displayed in Fig. 5 and Table-3, dithiocarbamate complex 1 has slightly higher χ value, whereas dithiocarbamate complex 2 has the lowest χ value.

The chemical potential (μ) is calculated as [$\mu = \frac{1}{2} (E_{\text{HOMO}} + E_{\text{LUMO}})$ -4.0763 eV, -3.9981 eV for complex 1 and 2 respectively], which is the opposite of chemical potential (μ). As shown in Table-3, the chemical potential (μ) value is the lower for the dithiocarbamate complex 2 and slightly higher for the dithiocarbamate complex 1. The calculated electrophilicity (ω)

values ($\omega = \mu^2/2\eta$ eV 4.3584 eV, 4.1586 eV for complex **1** and **2**, respectively), which was defined by Maynard *et al.* [40]. The electrophilicity (ω) value represents reduction in energy caused by maximum electron flow between an acceptor and a donor. Table-3 reveals that the electrophilicity (ω) value for the dithiocarbamate complex **1** is the slightly higher, whereas complex **2** is the lower. Electrophilicity (ω) is considered to be good if the chemical potential (μ) value is high and global hardness is low [41].

Molecular electrostatic potential (MEP): Molecular electrostatic potential diagram provides very valuable information for understanding of the chemical reactivity behaviour of molecular structure for medicinal significant molecules. The molecular electrostatic potential surface analysis of the complexes was determined by the DFT calculation using the optimized structures with B3LYP theory measure with LANL2DZ base set. The colours on the molecular electrostatic potential of the molecular structure indicate the electron-poor region with the

blue colour (positive electrostatic potential region for the electrophilic attack reactions) [42] and the electron-rich region with the red colour (negative electrostatic potential region for the nucleophilic attack reactions). The red colour on the molecular electrostatic potential is commonly related to the lone pair of the electronegative atom while the blue colour on the molecular electrostatic potential is related to the electropositive atom or group such as hydrogen atom. The regions between positive and negative potentials are represented by different colours, including green, yellow and orange. Green colour in the MEP surface indicates the neutral, zero electrostatic potential region showing hydrogen bonding interactions in the molecules. The electron density values of the complexes lies in the range of $-4.038 e^{-2}$ (negative site of the complex) to $+4.038 e^{-2}$ (positive site of the complex) and of $-3.446 e^{-2}$ to $+3.446 e^{-2}$ for complexes **1** and **2**, respectively.

The reactive sites for nucleophilic and electrophilic attack for dithiocarbamate complexes **1** and **2** are shown in Fig. 6. In

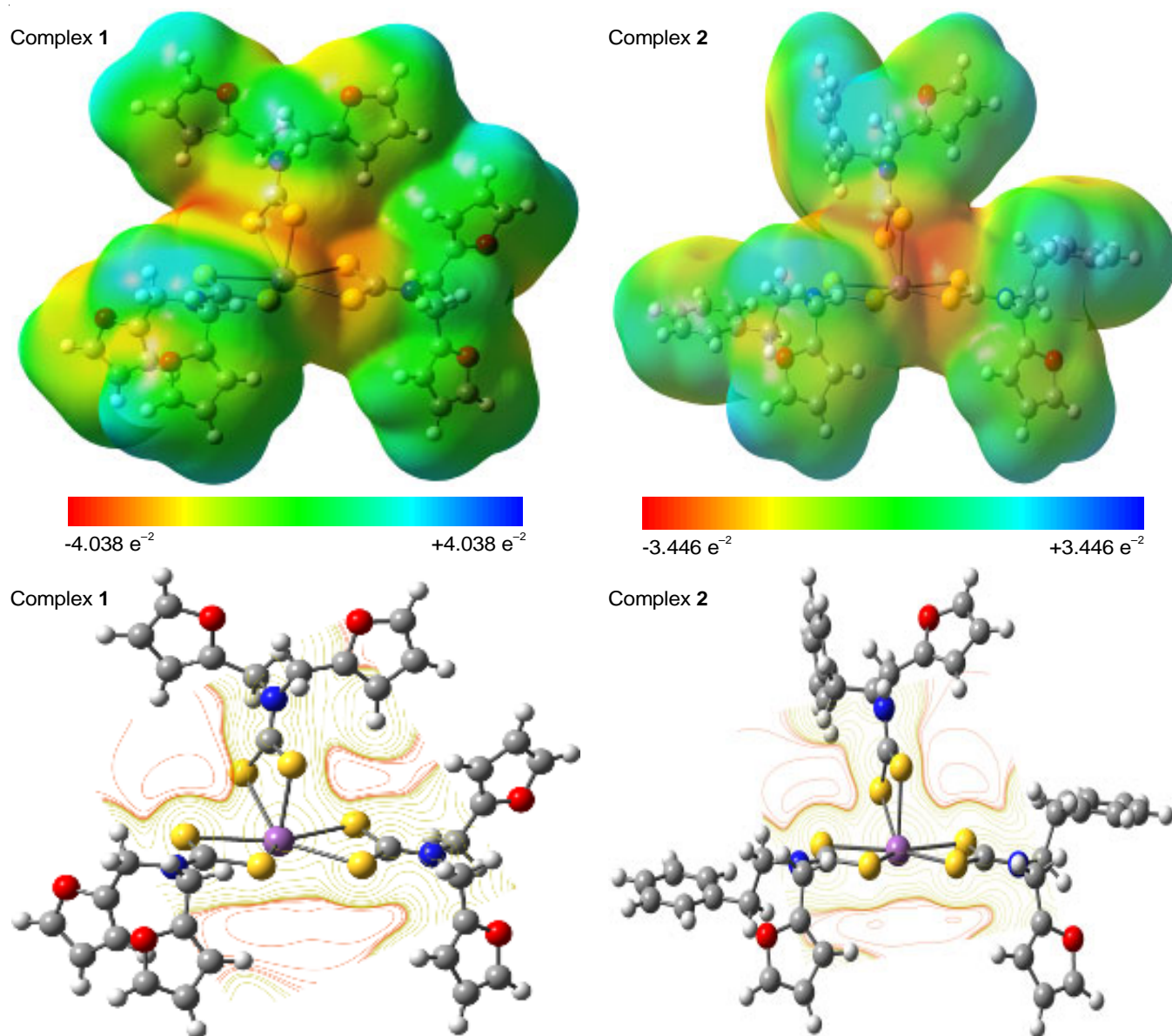


Fig. 6. Molecular electrostatic potential surface and contour of complexes **1** and **2**

the molecular electrostatic potential, the negative electrostatic potential regions are localized over the electronegative atoms such as oxygen, nitrogen and the positive electrostatic potential regions are localized over the hydrogen atoms. But sulphur atom of the complexes is less negative potential region than the other electronegative atoms such as oxygen and nitrogen. Therefore, the more positive electrostatic potential region and more negative electrostatic potential region sites are more favourable for the attraction of electrophilic and nucleophilic. The contour maps are a two dimensional show of the regions where the values of the virtual electron density lie within a range. The electron rich lines (red) are around oxygen and nitrogen whereas electron deficient lines are shown by greenish-yellow lines. The contour map surface displayed in Fig. 6 and calculated by same LANL2DZ basis sets at 0.004 density with same level of calculation of the molecular electrostatic potential mapped surface of the complexes. The contour images are used to show lines of stable brightness, such as molecular electrostatic potentials (MEP) and are drawn in the molecular plane.

Mulliken charge distribution: Mulliken and natural population analysis plays a very significant role in the application of quantum chemical calculation to molecular because atomic charges affect molecular polarizability, dipole moment, electronic structure and a lot of properties of molecular systems [43]. It is also used to be familiar with the charge distribution over the chemical bonding suggest, the formation of acceptor and donor pairs involving charge transfer in the molecule, the localization of negative and positive region in the molecular space, at which the electrons and proton concentrate, such as bond or lone pairs can be identified. It also discusses the processes of charge transfer in chemical reactions and electronegativity equalization.

Mulliken atomic charges of antimony complexes **1** and **2** were calculated using the B3LYP theory computed with LANL2DZ basis set. The total atomic charges of the complexes are indicated in Tables 4 and 5. The Mulliken atomic charges

on C atoms were exhibited either negative (C21 = -0.43652) or positive (C27 = 0.41352) value. Some carbon atoms have a maximum positive charge of C76 (0.490 for complex **2**), C64 (0.415 for complex **1**). All the H atoms were displayed a net positive charge in both complexes, but H31 = 0.2776 and H40 = 0.2788 for complex **1** and **2**, respectively were gained maximum positive charge than other hydrogen atoms in both complexes due to the presence of electronegative atoms such as oxygen and nitrogen. Mulliken total atomic charge analysis of complexes **1** and **2** are given in Fig. 7.

Antimicrobial activity: The antimony dithiocarbamate complexes assessed for their antimicrobial activity against four bacteria stains and two fungal organisms at a concentration of 400 and 800 µg/disc by disc diffusion process [44]. The dithiocarbamate complexes showed moderate to excellent antimicrobial activity against the Gram-negative (*Escherichia coli* and *Staphylococcus aureus*) and Gram-positive bacteria strains (*Klebsiella pneumoniae* and *Vibrio cholera*) and fungi organisms (*Aspergillus niger* and *Candida albicans*). The activity of the antimony complexes were compared to ciprofloxacin as standard drug. Antimicrobial activities of the antimony dithiocarbamate complexes are lower than those of the standard drug used. Table-6 indicates the various concentration of antimony complexes; dosage from 400 to 800 µg/disc, the antimicrobial action was increased. Both antimony dithiocarbamate complexes exhibited moderate activity against *Escherichia coli*, *Klebsiella pneumoniae* and slightly higher activity against *Staphylococcus aureus* and *Vibrio cholera*. The inhibitory activity of antimony complex **1** was greater against *Staphylococcus aureus* than those of complex **2**, because of electron withdrawing group, which increase the inhibitory activity of antibacterial.

The antifungal activities of antimony dithiocarbamate complexes were studied and results are summarized in Table-6. The antifungal activity of the complexes as compared with that of reference drug (ciprofloxacin). Complex **1** was higher active against *A. niger* and lower active against *C. albicans*.

TABLE-4
MULLIKEN ATOMIC CHARGE OF COMPLEX 1

Atom	Charge	Atom	Charge	Atom	Charge	Atom	Charge
Sb1	0.915444	C21	-0.43652	C41	-0.22695	C61	-0.15901
S2	-0.16779	C22	-0.48868	H42	0.28652	H62	0.247335
S3	-0.11615	H23	0.269001	C43	-0.1728	H63	0.254619
S4	-0.0852	C24	-0.42663	H44	0.253495	C64	0.415659
S5	-0.08084	H25	0.232108	H45	0.25758	C65	-0.37684
S6	-0.16744	H26	0.234566	H46	0.271059	O66	-0.29067
S7	-0.06961	C27	0.413529	H47	0.24308	C67	-0.24451
N8	0.006445	C28	-0.38849	C48	0.407494	H68	0.274043
N9	0.017453	O29	-0.28501	C49	-0.37966	C69	-0.15222
N10	0.030114	C30	-0.25301	O50	-0.2891	H70	0.252046
C11	-0.42309	H31	0.277688	C51	-0.24742	H71	0.257361
C12	-0.43153	C32	-0.14785	H52	0.274346	C72	0.335134
H13	0.262357	H33	0.252726	C53	-0.15296	C73	-0.3577
C14	-0.47331	H34	0.258201	H54	0.250959	O74	-0.27151
H15	0.271658	H35	0.267874	H55	0.257589	C75	-0.25677
C16	-0.40306	H36	0.272205	C56	0.369397	H76	0.266822
C17	-0.45658	H37	0.270831	C57	-0.34748	C77	-0.16546
H18	0.264377	C38	0.337521	O58	-0.27866	H78	0.253063
C19	-0.479	C39	-0.36261	C59	-0.26187	H79	0.258466
H20	0.244934	O40	-0.27493	H60	0.263823		

TABLE-5
MULLIKEN ATOMIC CHARGE OF COMPLEX 2

Atom	Charge	Atom	Charge	Atom	Charge	Atom	Charge
Sb1	0.917139	H25	0.182352	O49	-0.28822	H73	0.21538
S2	-0.17398	H26	0.233642	C50	-0.24498	H74	0.218009
S3	-0.10852	C27	-0.43097	H51	0.275232	H75	0.220289
S4	-0.10691	C28	-0.48807	C52	-0.15137	C76	0.490835
S5	-0.07866	H29	0.270495	H53	0.252179	C77	-0.40854
S6	-0.17469	C30	-0.37878	H54	0.258	C78	-0.38645
S7	-0.11426	H31	0.218643	H55	0.269604	C79	-0.21789
N8	0.039688	C32	-0.49526	H56	0.226051	H80	0.223758
N9	0.040196	H33	0.213491	C57	0.40326	C81	-0.22032
N10	0.039944	H34	0.2302	C58	-0.37729	H82	0.243109
C11	-0.43587	H35	0.228918	O59	-0.28916	C83	-0.23432
C12	-0.39399	C36	0.408833	C60	-0.24641	H84	0.216951
H13	0.248234	C37	-0.37298	H61	0.276555	H85	0.219117
C14	-0.49045	O38	-0.29678	C62	-0.15356	H86	0.221614
H15	0.180825	C39	-0.24688	H63	0.250969	C87	0.489019
H16	0.230735	H40	0.278876	H64	0.256942	C88	-0.4069
C17	-0.4806	C41	-0.15593	C65	0.484894	C89	-0.38915
H18	0.271199	H42	0.251222	C66	-0.40674	C90	-0.21904
C19	-0.40767	H43	0.256251	C67	-0.39602	H91	0.223847
C20	-0.49264	H44	0.262682	C68	-0.21805	C92	-0.21977
H21	0.269825	H45	0.26987	H69	0.230419	H93	0.245037
C22	-0.39312	H46	0.233602	C70	-0.21931	C94	-0.23487
H23	0.249187	C47	0.403846	H71	0.243947	H95	0.216466
C24	-0.49014	C48	-0.37026	C72	-0.2358	H96	0.218985
						H97	0.221193

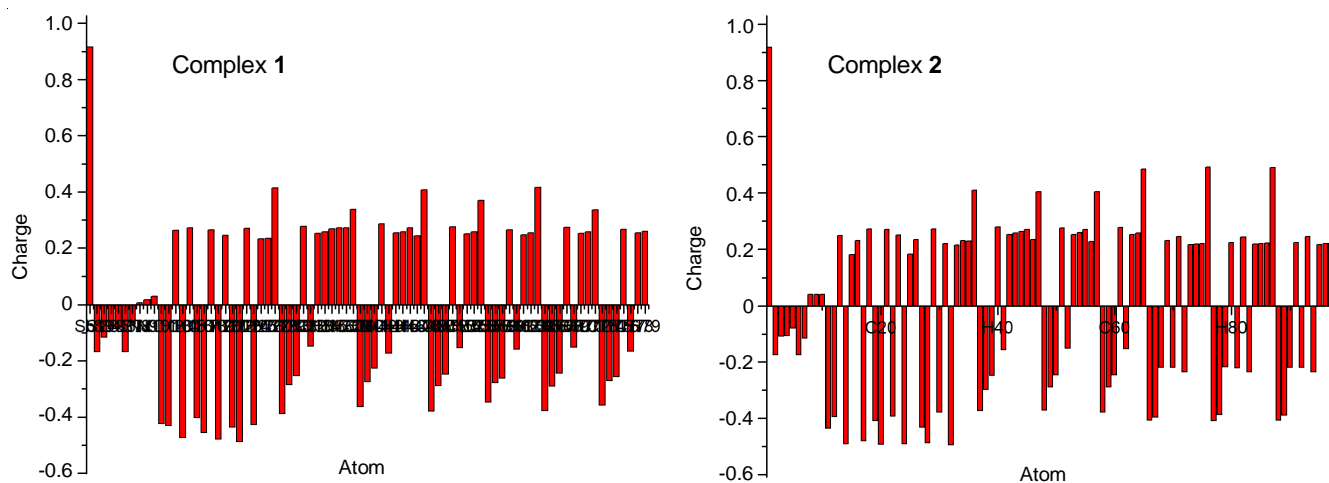


Fig. 7. Mulliken atomic charge analysis of complexes 1 and 2

TABLE-6
SUMMARY OF ANTIMICROBIAL SCREENING OF COMPLEXES 1 AND 2

Complex No.	Disc content (μg)	Selected bacteria				Selected fungal	
		<i>V. cholera</i>	<i>S. aureus</i>	<i>K. pneumoniae</i>	<i>E. coli</i>	<i>C. albicans</i>	<i>A. niger</i>
1	400	07	08	05	06	03	07
	800	14	16	13	12	07	14
2	400	06	07	06	07	06	05
	800	13	15	12	13	10	12
Ciprofloxacin		35	27	35	36	36	27

Conclusion

Two furfuryl based complexes *viz.* *tris(N,N*-difurfuryl-dithiocarbamato-S,S')antimony(III) (**1**) and *tris(N*-furfuryl-*N*-(2-phenylethyl)dithiocarbamato-S,S')antimony(III) (**2**) have

been synthesized and characterized by elemental analysis, FT-IR, ^1H NMR, ^{13}C NMR spectra, antimicrobial and theoretical studies. The IR spectra of antimony dithiocarbamates features three distinguishing bands, mainly associated with the stret-

ching vibrational bands. The aromatic protons signals are observed in the downfield regions in the range 6.31-7.30 ppm, which were theoretically observed in the range 6.2633-7.4144 ppm for complex **2**. The ^{13}C NMR spectra shows a signals at δ 204.1 ppm and δ 202.9 ppm, which were found at δ 229.2841 and δ 226.9378 ppm due to the thioureide carbon using the gauge-invariant atomic orbital (GIAO) method for complexes **1** and **2**, respectively. The C-N (thioureide) and C-S bond distances in the structure of dithiocarbamate complex **1** lies between 1.3517-1.3586 Å (C16-N9, C21-N10) and 1.75490-1.8294 Å (C16-S5, C16-S4). The calculated energy gap values 3.8125 and 3.8438 eV for complexes **1** and **2**, respectively. Molecular electrostatic potential (MEP) increase in the order of red < orange < yellow < green < blue. Green colour in the MEP surface indicates the neutral, zero electrostatic potential region showing hydrogen bonding interactions in the molecules. The Mulliken atomic charges on C atoms were exhibited either negative (C21 = -0.43652) or positive (C27 = 0.41352) value. Some carbon atoms have a maximum positive charge of C76, C64. The dithiocarbamate complexes showed moderate to excellent antimicrobial activity against the Gram-negative (*Escherichia coli* and *Staphylococcus aureus*) and Gram-positive bacteria strains (*Klebsiella pneumoniae* and *Vibrio cholera*) and fungi organisms (*Aspergillus niger* and *Candida albicans*).

CONFLICT OF INTEREST

The authors declare that there is no conflict of interests regarding the publication of this article.

REFERENCES

- G. Hogarth, *Mini Rev. Med. Chem.*, **12**, 1202 (2012); <https://doi.org/10.2174/138955712802762095>
- L.A. Ramos and E.T.G. Cavalheiro, *Braz. J. Therm. Anal.*, **2**, 38 (2013); <https://doi.org/10.18362/bjta.v2i1.11>
- A. Ramos-Espinosa, H. Valdes, M. Teresa Ramirez-Apan, S. Hernández-Ortega, B. Adriana Aguilar-Castillo, R. Reyes-Martínez, J. Manuel Germán-Acacio and D. Morales-Morales, *Inorg. Chim. Acta*, **466**, 584 (2017); <https://doi.org/10.1016/j.ica.2017.07.035>
- A. Jayaraju, K. Rameshbabu and J. Sreeramulu, *Int. J. Pharm. Pharm. Sci.*, **4**, 241 (2015).
- X. Hou, X. Li, H. Hemit and H.A. Aisa, *J. Coord. Chem.*, **67**, 461 (2014); <https://doi.org/10.1080/00958972.2014.890717>
- F. Shaheen, A. Badshah, M. Gielen, M. Dusek, K. Fejfarova, D. de Vos and B. Mirza, *J. Organomet. Chem.*, **692**, 3019 (2007); <https://doi.org/10.1016/j.jorganchem.2007.03.019>
- O. Guzel and A. Salman, *Bioorg. Med. Chem.*, **14**, 7804 (2006); <https://doi.org/10.1016/j.bmc.2006.07.065>
- F.F. Bobinihi, D.C. Onwudiwe, A.C. Ekennia, O.C. Okpareke, C. Arderne and J.R. Lane, *Polyhedron*, **158**, 296 (2019); <https://doi.org/10.1016/j.poly.2018.10.07>
- T. Zitouni, G. Ozkay, Y. Ozdemir, A. Asim, K. Zafer and D.A. Mehlika, *Lett. Drug Des. Discov.*, **8**, 830 (2011); <https://doi.org/10.2174/157018011797200786>
- A. Golcu, *Transition Met. Chem.*, **31**, 405 (2006); <https://doi.org/10.1007/s11243-006-0009-1>
- S. Khan, S.A.A. Nami and K.S. Siddiqi, *J. Organomet. Chem.*, **693**, 1049 (2008); <https://doi.org/10.1016/j.jorganchem.2007.12.026>
- S. Nagata, X. Zhou and H. Okamura, Antagonistic and Synergistic Effects of Antifouling Chemicals in Mixture; In: Encyclopedia of Ecology, Five-Volume Set; Elsevier: Amsterdam, The Netherlands, pp. 194-203 (2008).
- A. Warshawsky, I. Rogachev, Y. Patil, A. Baszkin, L. Weiner and J. Gressel, *Langmuir*, **17**, 5621 (2001); <https://doi.org/10.1021/la010299e>
- R. Ghorbani-Vaghei, M. Amiri and H. Veisi, *Bull. Korean Chem. Soc.*, **33**, 4047 (2012); <https://doi.org/10.5012/bkcs.2012.33.12.4047>
- R.M. Desai, D.K. Dodiya, A.R. Trivedi and V.H. Shah, *Med. Chem. Res.*, **17**, 495 (2008); <https://doi.org/10.1007/s00044-008-9093-4>
- C.J. Van Leeuwen, J.L. Maas-Diepeveen, G. Niebeek, W.H.A. Vergouw, P.S. Griffioen and M.W. Luijken, *Aquat. Toxicol.*, **7**, 145 (1985); [https://doi.org/10.1016/S0166-445X\(85\)80002-3](https://doi.org/10.1016/S0166-445X(85)80002-3)
- S.R. Thomas, H. Salahifar, R. Mashima, N.H. Hunt, D.R. Richardson and R. Stocker, *J. Immunol.*, **166**, 6332 (2001); <https://doi.org/10.4049/jimmunol.166.10.6332>
- F. Ozkanli, A.G. Usanmaz, K. Ozadali, E. Yildirim and K. Erol, *J. Pharm. Sci.*, **35**, 19 (2010).
- S.J. Hosseinimehr, D. Beiki, A. Kebriaeezadeh, A. Khalaj, M.P. Hamedani, S. Akhlaghpour, H. Esmaeili and A.R. Barazesh, *Iran. J. Radiat. Res.*, **7**, 91 (2009).
- S.T. Byrne, P. Gu, J. Zhou, S.M. Denkin, C. Chong, D. Sullivan, J.O. Liu and Y. Zhang, *Antimicrob. Agents Chemother.*, **51**, 4495 (2007); <https://doi.org/10.1128/AAC.00753-07>
- F.U. Shah, S. Glavatskih and O.N. Antzutkin, *Tribol. Lett.*, **45**, 67 (2012); <https://doi.org/10.1007/s11249-011-9855-x>
- R. Sarin, A.K. Gupta, D. Tuli, A.S. Verma, M.M. Rai and A.K. Bhatnagar, *Tribol. Int.*, **26**, 389 (1993); [https://doi.org/10.1016/0301-679X\(93\)90077-E](https://doi.org/10.1016/0301-679X(93)90077-E)
- J.O. Adeyemi and D.C. Onwudiwe, *Molecules*, **23**, 2571 (2018); <https://doi.org/10.3390/molecules23102571>
- P.J. Rani and S. Thirumaran, *Eur. J. Med. Chem.*, **62**, 139 (2013); <https://doi.org/10.1016/j.ejmech.2012.12.047>
- J.O. Adeyemi and D.C. Onwudiwe, *Molecules*, **25**, 305 (2020); <https://doi.org/10.3390/molecules25020305>
- M.A. Mumit, T.K. Pal, M.A. Alam, M.A. Islam, S. Paul and M.C. Sheikh, *J. Mol. Struct.*, **1220**, 128715 (2020); <https://doi.org/10.1016/j.molstruc.2020.128715>
- R. Ditchfield, *J. Chem. Phys.*, **56**, 5688 (1972); <https://doi.org/10.1063/1.1677088>
- K. Wolinski, J.F. Hinton and P. Pulay, *J. Am. Chem. Soc.*, **112**, 8251 (1990); <https://doi.org/10.1021/ja00179a005>
- H. Chermette, *J. Comput. Chem.*, **20**, 129 (1999); [https://doi.org/10.1002/\(SICI\)1096-987X\(19990115\)20:1<129::AID-JCC13>3.0.CO;2-A](https://doi.org/10.1002/(SICI)1096-987X(19990115)20:1<129::AID-JCC13>3.0.CO;2-A)
- K. Ramirez-Balderrama, E. Orrantia-Borunda and N. Flores-Holguin, *J. Theor. Comput. Chem.*, **16**, 1750019 (2017); <https://doi.org/10.1142/S0219633617500195>
- A. Zainuri, S. Arshad, N.C. Khalib and I.A. Razak, *Mol. Cryst. Liq. Cryst.*, **650**, 87 (2017); <https://doi.org/10.1080/15421406.2017.1328222>
- K. Chaturvedi, A. Kumar and A. Mishra, *Der Pharma Chem.*, **6**, 27 (2014).
- F. Bonati and R. Ugo, *J. Organomet. Chem.*, **10**, 257 (1967); [https://doi.org/10.1016/S0022-328X\(00\)93085-7](https://doi.org/10.1016/S0022-328X(00)93085-7)
- A.W. Herlinger, S.L. Wenhold and T.V. Long II, *J. Am. Chem. Soc.*, **92**, 6474 (1970); <https://doi.org/10.1021/ja00725a015>
- H.L.M. Van Gaal, J.W. Diesveld, F.W. Pijpers and J.G.M. Van der Linden, *Inorg. Chem.*, **18**, 3251 (1979); <https://doi.org/10.1021/ic50201a062>
- R.V. Solomon, P. Veerapandian, S.A. Vedha and P. Venuvanalingam, *J. Phys. Chem. A*, **116**, 4667 (2012); <https://doi.org/10.1021/jp302276w>
- A. Prasad, S.K. Kalainathan and S.P. Meenakshisundaram, *Optik*, **127**, 6134 (2016); <https://doi.org/10.1016/j.ijleo.2016.04.060>
- T.A. Koopmans, *Physica*, **1**, 104 (1934); [https://doi.org/10.1016/S0031-8914\(34\)90011-2](https://doi.org/10.1016/S0031-8914(34)90011-2)
- R.S. Mulliken, *J. Chem. Phys.*, **2**, 782 (1934); <https://doi.org/10.1063/1.1749394>
- R.G. Parr, L. Szentpály and S. Liu, *J. Am. Chem. Soc.*, **121**, 1922 (1999); <https://doi.org/10.1021/ja983494x>
- A. Kumar, R. Kumar, A. Gupta, P. Tandon and E.D. D'silva, *J. Mol. Struct.*, **1150**, 166 (2017); <https://doi.org/10.1016/j.molstruc.2017.08.072>
- R.K. Singh, S.K. Verma and P.D. Sharma, *Int. J. Chemtech Res.*, **3**, 1571 (2011).
- I. Rajaei and S.N. Mirsattari, *J. Mol. Struct.*, **1163**, 236 (2018); <https://doi.org/10.1016/j.molstruc.2018.02.010>
- H.P.S. Chauhan and U.P. Singh, *Appl. Organomet. Chem.*, **21**, 880 (2007); <https://doi.org/10.1002/aoc.1290>